Magnetic-Based Positioning System for Moving Target With Feature Vector

Y. ZHENG[1,2], Q. LI[1], C. WANG[1], X. LI[1], AND Y. HUANG[3]

[1]Research Center of Space Control and Inertial Technology, Harbin Institute of Technology, Harbin 150001, China
[2]Harbin Electric Machinery Company Ltd., Harbin 150001, China
[3]China National Nuclear Corporation, Nuclear Power Operations Management Co., Ltd., Haiyan 314300, China

Corresponding author: C. Wang (cwang@hit.edu.cn)

ABSTRACT Underground, indoor, and harsh environments, which are complex, mutable, and hard to model, prevent high accuracy positioning and navigation. In this paper, a novel positioning system suitable to such environments is proposed. This system is based on a magnetic feature vector integrated with a miniature inertial measurement unit (MIMU). Compared with traditional magnetic-based positioning systems (MBPS), the proposed system exhibits better robustness, and applicability, which is proved by experimental results. Its non-accumulated error characteristics and outstanding penetrability enable the system to provide long-time accurate position and attitude service in underground, indoor, and harsh environments. The experiments indicate that the expected precision of the system can reach 0.055 and 0.062 m and an angle error of 2.1° and 2.8° in line of sight (LOS) and non-line of sight (NLOS) environments, respectively, in the static experiment and 0.051 m in the moving target tracking experiment.

INDEX TERMS Integrated navigation, magnetic application on positioning and attitude, MIMU, moving target tracking.

I. INTRODUCTION

GPS is known as the most popular system for navigation and positioning. However, its use is impossible in some overbuild or blocked environments, such as indoor environments due to multipath effects, location, and navigation in indoor areas are hard to achieve. Recently, the development of indoor positioning systems has attracted significant attention. Technologies, such as Ultra-Wide Band (UWB) [1], [2], Image Recognition-Based Positioning (IRBP) [3], radio frequency identification (RFID) [4], and lasers [5]) have been investigated.

The magnetic-based positioning method has attracted significant interest for indoor location and navigation [6]–[17] because it is less sensitive to propagation-dependent disturbances, penetration, and multipath effects compared to radio frequency (RF)-based methods. The propagation of the magnetic field is a complex process. It depends not only on the medium but also on the frequency and the power of the magnetic field. The medium and the power should be

the main factors that affect the propagation distance of the magnetic field. However, in the same condition, generally speaking, the lower frequency magnetic field has a larger wavelength than the higher one, which makes it through more obstacles.

In an earlier study [6], a direct current (DC) artificially generated magnetic system was investigated. Similar works were presented earlier [7], [8]. In these studies, a fitting line of the magnetic intensity decay with the distance between the receiver and magnetic beacon (MB) was applied, which might be disturbed easily. Furthermore, high quality magnetic sensors are required to provide effective coverage within 18 m. To address these issues, a system with a low frequency alternating current signal was considered, which provides a balance between the propagation distance, and immunity [9]. Many related works focusing on magnetic ranging [10]–[14], magnetic fingerprints positioning [15], [16], and attitude estimation [17], [18] have been proposed as guidance.

Wu *et al.* [14] presented a novel idea that the step-frequency signal is employed as the driving signal to track the optimal resonant frequency, which will maximize the transmission power of two resonant coils. Magnetic fingerprints

---

The associate editor coordinating the review of this manuscript and approving it for publication was Wuliang Yin.

positioning is investigated popularly. Tang *et al.* [15] used WLAN RSS fingerprint and magnetic field fingerprint to improve fingerprint's spatial and time characterization and localization accuracy. Chen *et al.* [16] proposed an indoor magnetic-based positioning model by learning sequence-based fingerprint from raw magnetic field sequences, which aimed to overcome the pattern embedded in raw magnetic field sequences that might be locally distorted or scaled. This greatly limits the positioning performance. The performance shows that MBPS is significant in the particular applying environment. The attitude measurement using a magnetometer meets the requirements of miniaturization, low power consumption, and low cost for the navigation system. Yu *et al.* [17] showed an attitude measurement method with magnetic sensors and high precise turntable, which yields outstanding results with an error of below 1° in the laboratory environment. The no-accumulated error of MBPS is also used to couple with miniature inertial measurement unit (MIMU) and correct the attitude and position error [12], [18].

However, many efforts have been made to improve the performance of MBPS. The magnetic ranging method is hard to be modeled accurately in the obscured and uncertain medium of some harsh environments. The actual magnetic descending gradient might be distorted compared to that represented by the model. Furthermore, the fitting line of the magnetic intensity and distance requires sufficient prior information of the magnetic field decay in the considered environment, which seriously constrains the application of this method. Although the method can measure the distance between the magnetic beacon and receiver, the related transformation angles (the attitude angles of the receiver) from the receiver to the MB are hard to be determined by the proposed methods.

In this paper, a method, which uses a magnetic feature vector with a low frequency magnetic field capable of providing position, and attitude solution, is proposed. This method exhibits better robustness and applicability on harsh environments, which are complex, mutable, and hard to model, than traditional methods. In [19] a constant vector related to the induced magnetic field and magnetic dipoles is described and a similar work is presented in [20]. Considering a low driving frequency and Shannon's sampling theorem, the time delay from different MBs may contribute to extra positioning errors in real time navigation of moving targets. These errors may be ignored for static targets. Aiming to solve this problem, a gravitation-based particle filter algorithm integrated with a MIMU is proposed. Thus, real time positioning using the proposed magnetic-based positioning system (MBPS) can be realized. The novelty of the proposed MBPS can be outlined as follows:

1. Compared with traditional MBPS with good penetrability of a low frequency magnetic field, the proposed MBPS exhibits better robustness and precision under the same conditions without the requirement of prior
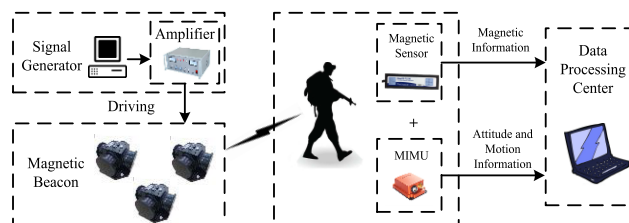

FIGURE 1. Block diagram of the proposed magnetic-based positioning system.

knowledge of the magnetic field decay. Thus, the proposed MBPS is more adaptable to practical applications.

2. The proposed MBPS can provide not only information on the position but also on the attitude of the receiver, which is not accumulated with time.

3. The time delay error caused by the low updating speed, which prevents the system from its application to tracking moving targets, can be solved by integrating a MIMU.

This paper is organized as follows: the necessity of the investigation and the main purpose of the proposed system are outlined in Section 1. In Section 2 the design of the proposed MBPS is introduced. The principle of the proposed gravitation-based particle filter algorithm and the integrated model of the proposed system are described in Section 3. Experiments are presented in Section 4 to validate the advantages of the proposed MBPS with respect to real time positioning accuracy. Finally, the conclusions are briefly presented in Section 5.

II. SYSTEM DESIGN

In this section, an overview of the system design of the proposed MBPS is presented. The system, which is shown in Fig. 1, is mainly composed of a signal generator, MBs, power amplifiers, a magnetic sensor and a MIMU sensor, and a data processing center.

Computers are used for the signal generator and the data processing center in our actual physical implementation. However, considering the code size and response speed, the data processing center can be replaced completely by a microprocessor. Sinusoidal signals of a certain frequency are generated by a digital-to-analog module according to the system computer clock and amplified by power amplifiers to drive the MBs. The requirement of the DA module is not strict, and only the direction of the magnetic feature vector defined in the paper is important to the positioning result. Small amplitude errors will not affect the direction result. The different frequencies mainly provide the feature that is required for distinguishing different magnetic beacons. Therefore, small frequency error is also acceptable only if the frequency can be distinguished. The amplifier has to have enough power to provide a stable current which supports to the effective coverage of the magnetic beacon. The reactance
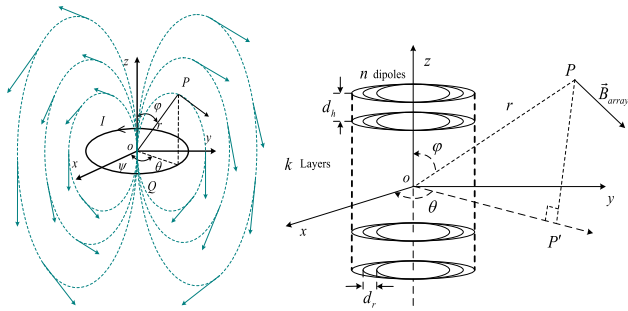
FIGURE 2. Models of magnetic diploe and magnetic beacon (MB).

generated by the MB is an important element. Using the magnetic sensor and the fast Fourier transform, corresponding information of the MB is extracted and processed by the data processing center. Generally, a more accurate magnetic sensor results into better performance. The magnetic sensor resolution applied in our system is 1nT.

Herein, the design of the MB and the MIMU integrated model are introduced.

A. MB DESIGN

A circular current loop [14], which is called magnetic dipole (MD), can be modeled as shown in Fig. 2. Assuming that the magnetic permeability is μ and the excited current is I, the magnetic moment $\vec{M}$ can be expressed as

$$\boldsymbol{M} = I \cdot S \cdot \boldsymbol{i} \tag{1}$$

Here, S represents the area of the current loop $\boldsymbol{i}$, which shows the direction that satisfies Fleming's right-hand rule. The direction of $\boldsymbol{i}$ shows the magnetic moment generated by a single MD.

According to the operation principle of MDs, the proposed MB is constructed by an MD array as shown in Fig. 2. Then, the induced magnetic field of the designed MB with k layers and n dipoles in each layer at a position $\boldsymbol{P} = (r, \varphi, \theta)$ can be represented as [15]

$$\boldsymbol{B}(r, \theta, \varphi) = \begin{cases} \sum\limits_{i=1}^{k} \sum\limits_{j=1}^{n} \dfrac{3\mu_0 I r^2 R_j^2 \sin 2\varphi \cos \theta}{4(R_j^2 + r^2 + h_i^2)^{\frac{5}{2}}} \\[3mm] \sum\limits_{i=1}^{k} \sum\limits_{j=1}^{n} \dfrac{3\mu_0 I r^2 R_j^2 \sin 2\varphi \sin \theta}{4(R_j^2 + r^2 + h_i^2)^{\frac{5}{2}}} \\[3mm] \sum\limits_{i=1}^{k} \sum\limits_{j=1}^{n} \dfrac{\mu_0 I R_j^2}{(R_j^2 + r^2 + h^2)^{\frac{3}{2}}} \\[3mm] \qquad [1 - \dfrac{3r^2 \sin^2 \varphi}{2(R^2 + r^2 + h^2)}] \end{cases} \tag{2}$$

Here, i and j represent the dipole at row i and column j in the upper half space; R_j is the radius of the n-th column MD, where $R_j = R_0 + (j-1) d_r$; h_i is the height of the i-th row relative origin o, where $h_i = h_0 + (i-1) d_h$.

According to a previous work [16], a simplified model can be expressed as follows

$$\boldsymbol{B}(r, \theta, \varphi) = \begin{bmatrix} B_x & B_y & B_z \end{bmatrix}^T$$

$$= \begin{bmatrix} \dfrac{3\mu M r^2 \sin 2\varphi \cos \theta}{4\pi \left(R_d^2 + r^2 + h_d^2\right)^{\frac{5}{2}}} \\[4mm] \dfrac{3\mu M r^2 \sin 2\varphi \sin \theta}{4\pi \left(R_d^2 + r^2 + h_d^2\right)^{\frac{5}{2}}} \\[4mm] \dfrac{\mu M}{2\pi \left(R_d^2 + r^2 + h_d^2\right)^{\frac{3}{2}}} \left[1 - \dfrac{3r^2 \sin^2 \varphi}{2 \left(R_d^2 + r^2 + h_d^2\right)}\right] \end{bmatrix} \tag{3}$$

Here, N_d is the equivalent number of turns, R_d is the equivalent radius, and h_d is the equivalent height. M and R_d can be calculated by

$$M = \pi R_d^2 N_d I$$

$$R_d = \sqrt{\frac{1}{n} \sum_{j=1}^{n} R_i^2}, \, h_d = \frac{1}{n} \sum_{i=1}^{k} h_i \tag{4}$$

The accuracy error of the model is less than 5%. This error decreases as the distance increases, which is verified in the near, and far magnetic field (within 5 m×5 m) experiment.

B. POSITION AND ATTITUDE DETEMINATION

According to (3), the definition of magnetic feature vector can be expressed as

$$\boldsymbol{v}_i = \boldsymbol{i}_i \tag{5}$$

wherein, $\boldsymbol{i}_i$ is the unit vector that points from the $i-th$ MB to the receiver $\boldsymbol{P}$ and can be presented as

$$\boldsymbol{i}_i = (\sin \varphi_i \cos \theta_i, \sin \varphi_i \sin \theta_i, \cos \varphi_i) \tag{6}$$

The angles of the unit vector $\boldsymbol{i}_i$ can be computed using (3) as the following equations:

$$h(\theta) = \tan \theta_i = \frac{B_y}{B_x}$$

$$h(\varphi) = \frac{6r^2 \sin 2\varphi_i}{4R_d^2 + r^2 + 4h_d^2 + 3r^2 \cos 2\varphi_i}$$

$$= \frac{\sqrt{(B_x)^2 + (B_y)^2}}{B_z} \tag{7}$$

Since the function $h(\varphi)$ is monotonous (this is proved in appendix 1), $\boldsymbol{v}_i$ can be uniquely determined by (7).

Theoretically, the position of the receiver can be estimated by two MBs according to the trigonometric positioning principle, which is shown in Fig.3. With the constant distance between the two MBs and the known attitude of the vector pointing to the receiver, the position can be determined by the only value.

The trigonometric positioning is based on the premise that coordinates can be unified, but it is hard to be realized in
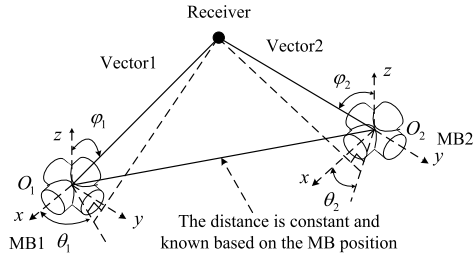
FIGURE 3. The principle of trigonometric positioning method.
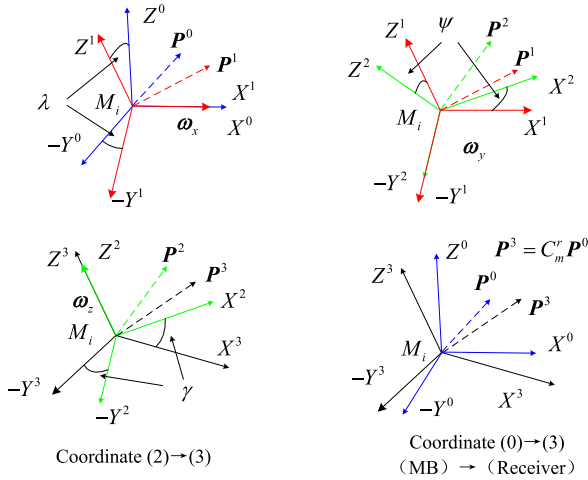
FIGURE 4. Transformation from the coordinate of the MB to that of the receiver.

FIGURE 5. Geometric principle of the proposed method.

the actual works for the attitude error of the receiver. Using the MIMU is a good solution to settle the attitude problem. But the random walk and accumulated error would make the positioning error increase with the time. In this paper, we proposed an improved feature vector method with three MBs which can provide the position and attitude information of the receiver.

It is assumed that there are three MBs that can provide the observed feature vector at the receiver position P. Considering the local coordinate of the receiver, c_r, and that of MB, c_m, have a transformation that there exists a rotation angle of λ, ψ, γ with x, y, z respectively. As shown in Fig. 4, the transformation can be denoted that

$$c_r = C_m^r c_m \qquad (8)$$

where

$$C_m^r = \begin{bmatrix} C_{11} & C_{12} & C_{13} \\ C_{21} & C_{22} & C_{22} \\ C_{31} & C_{32} & C_{33} \end{bmatrix} \qquad (9)$$

$C_{11} = \cos(\gamma)\cos(\psi), C_{21} = \sin(\gamma)\cos(\psi)$

$C_{31} = -\sin(\psi)$

$C_{12} = \cos(\gamma)\sin(\psi)\sin(\lambda) - \sin(\gamma)\cos(\lambda)$

$C_{22} = \sin(\gamma)\sin(\psi)\sin(\lambda) + \cos(\gamma)\cos(\lambda)$

$C_{32} = \cos(\psi)\sin(\lambda)$

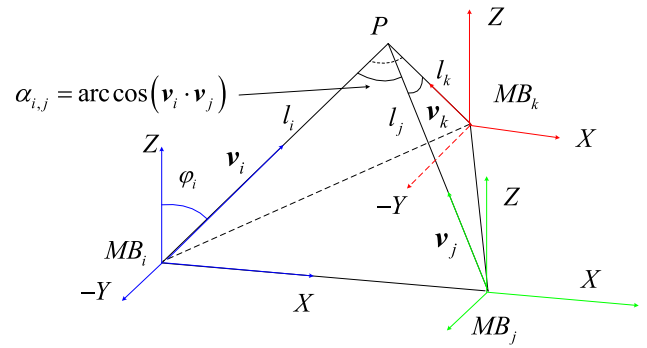$C_{13} = \cos(\gamma)\sin(\psi)\cos(\lambda) + \sin(\gamma)\sin(\lambda)$

$$C_{23} = \sin(\gamma)\sin(\psi)\cos(\lambda) - \cos(\gamma)\sin(\lambda)$$
$$C_{33} = \cos(\psi)\cos(\lambda) \qquad (10)$$

Therefore, the feature vector $v_i = (v_{ix}, v_{iy}, v_{iz})$ in c_m and $v'_i = (v'_{ix}, v'_{iy}, v'_{iz})$ in c_r has the relation

$$v'_i = C_b^n v_i \qquad (11)$$

Therefore, it can be easily proved that the angle α'_{ij} between the vectors v'_i and v'_j is equal to α_{ij} between v_i and v_j, which is not related to the attitude of the receiver. The verification is given in appendix II. Therefore, the angle of the two feature vectors can be expressed as

$$\cos\alpha_{ij} = (v'_i \cdot v'_j) = (v_i \cdot v_j) \qquad (12)$$

Then, as shown in Fig. 5, the distance between the receiver and the MBs can be computed as

$$l_{ij}^2 = l_i^2 + l_j^2 - 2l_i l_j \cos\alpha_{ij} \qquad (13)$$

Herein, l_{ij} presents the distance between the $i - th$ and $j - th$ MBs, which can be known by prior information, α_{ij} can be measured by the feature vectors v'_i and v'_j, and the distance l_i between P and $M_i = \left(m_x^{(1)}, m_y^{(1)}, m_z^{(1)}\right)$ can be solved by at least three MBs.

According to the solutions of (13), $P = (p_x, p_y, p_z)$ can be solved by equations

$$l_i = \left\| (p_x, p_y, p_z) - \left(m_x^{(i)}, m_y^{(i)}, m_z^{(i)}\right) \right\|, \quad (i = 1, 2, 3) \qquad (14)$$

Furthermore, with the solution of P, the feature vector in c_m can be estimated as

$$\hat{v}_i = \frac{\hat{P} - M_i}{\hat{l}_i} \qquad (15)$$

Herein, $\hat{P}$ is the estimated position of the receiver based on (12) and $\hat{l}_i$ is the related estimation based on (14). Therefore, the transforming matrix C_b^n has the relation between the measured feature vector v'_i according to (9)

$$v'_i = C_m^r \hat{v}_i. \qquad (16)$$

Thus, the transforming matrix can be solved by at least three MBs i, j, k
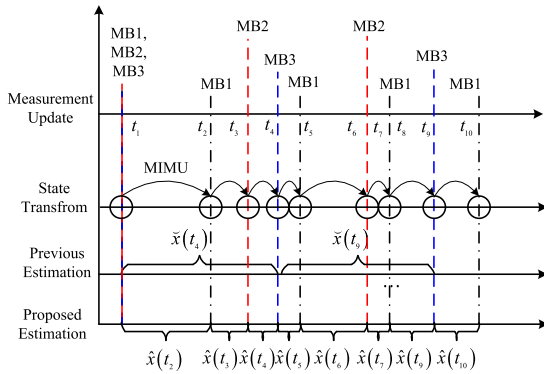
$$C_b^n = BA^T \left(AA^T\right)^{-1}, \qquad (17)$$

FIGURE 6. Comparison of processes in the proposed method.

where

$$A = \begin{bmatrix} \hat{v}_i, \hat{v}_j, \hat{v}_k \end{bmatrix} \quad \text{and } B = \begin{bmatrix} v'_i, v'_j, v'_k \end{bmatrix}. \quad (18)$$

Finally, the attitude angles λ, ψ, γ can be computed by the equations

$$\begin{cases} \psi = \arcsin(-C_{31}) \\ \gamma = \arctan\left(\dfrac{C_{21}}{C_{11}}\right) \\ \lambda = \arctan\left(\dfrac{C_{32}}{C_{33}}\right). \end{cases} \quad (19)$$

The real values of λ, ψ, γ can be found in the real value table in [26]. Notice that the estimated error of P influences the error of λ, ψ, γ. We will not elaborate on this further here.

C. INTEGRATED SYSTEM MODEL
In the previous section, it has been proved that the MBPS is able to provide the position and attitude information independently without accumulated error. However, one disadvantage of the MBPS is the low updating speed of the measurement caused by the low frequency magnetic field signal, which exhibits strong penetrability. In static target tracking cases, this is acceptable. However, in moving target tracking cases, the time delay measurement between two MBs will contribute to estimation errors and the low updating speed may lead to state loss, especially for high mobility targets. Therefore, a MIMU can be added to solve the time delay problem and compensate for the state loss between two updating time points of the MBPS.

According to Fig. 6, the updating speed of the MBPS can be improved by making full use of each sampling time MB1 and MB2 are assumed once updated with 5 sampling periods and 8 sampling periods, respectively. The previous estimation uses the max period of signals as the data update period. Therefore, the previous estimation updating times in Fig. 6 are at t_3, t_6, t_9. The measurement at t_3 is the average value within the time interval $[t_1, t_3]$. If we assume the time $t = t_3 - t_1$ is 0.05 s (assuming the updating frequency of MB_1 and MB_2 to be 20 Hz and 30 Hz, respectively, and a velocity of 10 m/s) and the estimation is unbiased, the positioning delay error may close to 0.17 m. Furthermore, for high-speed moving targets, the state of $x(t_5), x(t_6), x(t_7), x(t_8)$ might

be missed, when the measured time of MB3 is used as the updating time between t_4 and t_9. Then, if the proposed algorithm is applied, the estimation updating times are $t_1, \ldots, t_{10}$. Thus, the delay error can be reduced. It is noted that the output of the MIMU is used to support the particle transformation between two sampling times $k - 1$ and k. If the time between sampling times $k - 1$ and k is very short, the drift error of the MIMU can be neglected. Furthermore, the error will be corrected by the update of the MBPS next time.

Let us assume that the state of the system is 15 dimensions [24], such as $x_k = \begin{bmatrix} \phi_k & \omega_k & r_k & v_k & a_k \end{bmatrix}^T$. Herein, ϕ_k is the attitude vector, ω_k represents the angular velocity vector, r_k is the position vector, v_k is the velocity vector, and a_k is the acceleration vector. The, the state transition equation can be expressed as

$$\begin{aligned} x_k &= F_{k,k-1} x_{k-1} + w_{k-1} \\ z_k &= H_k x_k + v_k \end{aligned} \quad (20)$$

Here, T_s is the sampling time of the MIMU

$$F_k = \begin{bmatrix} I_{3\times3} & T_s \cdot C_b^n & O_{3\times3} & O_{3\times3} & O_{3\times3} \\ O_{3\times3} & I_{3\times3} & O_{3\times3} & O_{3\times3} & O_{3\times3} \\ O_{3\times3} & O_{3\times3} & I_{3\times3} & I_{3\times3} & O_{3\times3} \\ -T_s \cdot S_t & O_{3\times3} & O_{3\times3} & I_{3\times3} & T_s \cdot C_b^n \\ O_{3\times3} & O_{3\times3} & O_{3\times3} & O_{3\times3} & I_{3\times3} \end{bmatrix} \quad (21)$$

and

$$S_t = \begin{bmatrix} 0 & -a_{kx}^n & a_{ky}^n \\ a_{kx}^n & 0 & -a_{kx}^n \\ -a_{ky}^n & a_{kx}^n & 0 \end{bmatrix} \quad (22)$$

$$H_k = \begin{cases} H_1 = \begin{bmatrix} I_{3\times3} & O_{3\times3} & O_{3\times3} & O_{3\times3} & O_{3\times3} \\ O_{3\times3} & O_{3\times3} & I_{3\times3} & O_{3\times3} & O_{3\times3} \end{bmatrix} \\ H_2 = \begin{bmatrix} O_{3\times3} & I_{3\times3} & O_{3\times3} & O_{3\times3} & O_{3\times3} \\ O_{3\times3} & O_{3\times3} & O_{3\times3} & I_{3\times3} & O_{3\times3} \\ O_{3\times3} & O_{3\times3} & O_{3\times3} & O_{3\times3} & I_{3\times3} \end{bmatrix} \end{cases} \quad (23)$$

When the MBPS has an output, the measured matrix is $H_k = \begin{bmatrix} H_1^T, H_2^T \end{bmatrix}^T$. Otherwise, $H_k = \begin{bmatrix} O_{6\times15}^T, H_2^T \end{bmatrix}^T$.

III. ESTIMATION OF THE MOVING TARGET POSITION
A. TIME DELAY OF THE MAGNETIC-BASED POSITIONING SYSTEM FOR TRACKING A MOVING TARGET
According to the Shannon's sampling theorem, a signal of at least two complete periods is required to ensure undistorted restoration of analog signals. For the low frequency induced magnetic signal, the sampling needs more time, which is contributed to the tracking time delay of the moving target. The sampling and measurement updates are described in Fig. 7.

For the very low frequency magnetic signal, the computation resource is surplus. Thus, the computational delay of the algorithm can be neglected and two different updating speeds for the measurement of the two MBs with different frequency can be used. This is shown in Fig. 7. Assuming that the frequencies of the induced magnetic field are 20Hz and 25Hz,
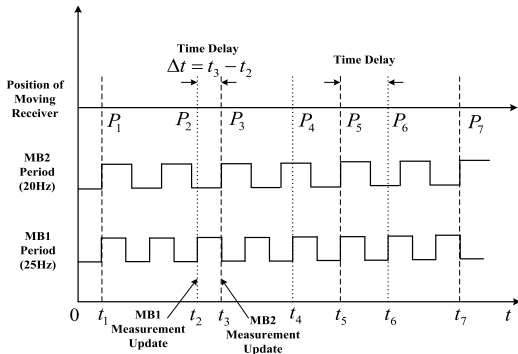
FIGURE 7. Time delay caused by different sampling frequencies.

respectively, the time delay $\Delta t = t_3 - t_2$ will reach 0.02s. Also, assuming that the velocity of the moving target is 4 m/s, the delay error may approach 8cm. It is noted that the delay error is additional to the MBPS inherent error. Considering that the positioning accuracy is close to 10cm, the 8cm delay error is very large. Moreover, with the frequency decreasing and velocity increasing, the time delay error will increase correspondingly.

Therefore, the use of two near sampling data points for the estimation of the receiver position will contribute to large positioning errors. Furthermore, the use of common multiple sampling data points also results in a very low updating speed, which is unsuitable to the multi-MBs case. This is because the frequency of the signal is very low and seriously affects a real time system Therefore, to improve the real time and reduce the time delay error, a gravitation-based particle filter algorithm is used. This algorithm is capable of estimating the moving target position by considering the nonlinear observation described in (5).

B. GRAVITATIONAL FIELD ALGORITHM PARTICLE FILTER(GFA-PF)

GFA-PF is a new heuristic search algorithm, which is based on the simulation of planetary formation processes. In the GFA-PF, a mobile factor able to drive the particles to approach a high likelihood region is proposed, so that the particles can concentrate rapidly in the nearby real state. It has been proved that the GFA-PF performs well on avoiding particle degradation and dilution in [25].

In the particle filter algorithm, the probability of a state particle $p(x_k | Y_k)$ based on the prior probability $p(x_k | Y_{k-1})$ can be presented as

$$p(x_k, x_{k-1} | Y_{k-1}) = p(x_k | x_{k-1}, Y_{k-1}) p(x_{k-1} | Y_{k-1}) \quad (24)$$

When x_{k-1} is determined, x_k and Y_{k-1} are mutually uncorrelated. Therefore, using an integral, (11) can be written as

$$p(x_k | Y_{k-1}) = \int p(x_k | x_{k-1}, Y_{k-1}) p(x_{k-1} | Y_{k-1}) dx_{k-1} \quad (25)$$

Thus, assuming that y_k is only determined by x_k, the posterior probability $p(x_k | Y_k)$ at time k can be calculated on the prior probability $p(x_k | Y_{k-1})$ at time k as

$$p(x_k | Y_k) = \frac{p(y_k | x_k) p(x_k | Y_{k-1})}{\int p(y_k | x_k, Y_{k-1}) dx_k} \quad (26)$$

The particle set can be written as $\left\{ x_k^{(j)}, \omega_k^{(j)} \right\}_{j=1}^N$, where $x_k^{(j)}$ is the $j-th$ state particle at time k. The corresponding weight is $\omega_k^{(j)}$. Therefore, the weight update equation can be rewritten as

$$\omega_k^{(j)} \propto p\left(y_k \left| x_k^{(j)} \right.\right) \omega_{k-1}^{(j)} \quad (27)$$

According to the theory described previously, three MB measurements are required to guarantee the stability of the estimation result. In Fig. 6, time t_4 is taken as an example. The measurement of MB3 at time t_4 is denoted as $y(t_4)$ and the latest measurements from the other two measurements at time t_3, t_2 are denoted as $y(t_3)$, $y(t_2)$. Then, the estimated error of the MB1 can be expressed as

$$\tilde{g}(x(t_2)) = g(x(t_2)) - \hat{g}(x(t_2)) \quad (28)$$

Herein, $g(\cdot)$ is the function obtained from (7), which can be expressed as

$$v_i = (\theta_i, \varphi_i) = g(x(t)) \quad (29)$$

Assuming $\tilde{g}(x(t_2))$ is not equal to a zero vector, the posterior probability of particle $x^{(j)}(t_2)$ based on the measurement of MB1 can be written as

$$p_1 = p\left(y(t_2) \left| x^{(j)}(t_2) \right.\right) \propto \frac{1}{trace\left(\tilde{g}^{(j)}(t_2)^T \tilde{g}^{(j)}(t_2)\right)} \quad (30)$$

The time delay problem between t_2 and t_3 can be solved by transforming the particles $\left\{ x^{(j)}(t_2) \right\}_{j=1}^N$ according to the measurement of the MIMU (9), which can be expressed as

$$\left\{ x^{(j)}(t_3) \right\}_{j=1}^N = F_{t_3, t_2} \cdot \left\{ x^{(j)}(t_2) \right\}_{j=1}^N \quad (31)$$

Since the time delay $\Delta t = t_3 - t_2$ is small enough for the MIMU, it is assumed that the transformation error can be ignored.

Then, the posterior probability of the state $x^{(j)}(t_3)$, which is based on the measurement of MB2, can be written as

$$p_2 = p\left(y(t_3) \left| x^{(j)}(t_3) \right.\right) \propto \frac{1}{trace\left(\tilde{g}^{(j)}(t_3)^T \tilde{g}^{(j)}(t_3)\right)} \quad (32)$$

Similarly, the posterior probability of the state $x^{(j)}(t_4)$ from the MB3 can be obtained from

$$p_3 = p\left(y(t_4) \left| x^{(j)}(t_4) \right.\right) \propto \frac{1}{trace\left(\tilde{g}^{(j)}(t_4)^T \tilde{g}^{(j)}(t_4)\right)} \quad (33)$$

Therefore, assuming that the initial weight of $x^{(j)}$ is $\omega^{(j)}(t_1)$, the relation for weight updating can be obtained

$$\omega^{(j)}(t_2) = p_1 \omega^{(j)}(t_1), \omega^{(j)}(t_3) = p_1 \omega^{(j)}(t_2),$$
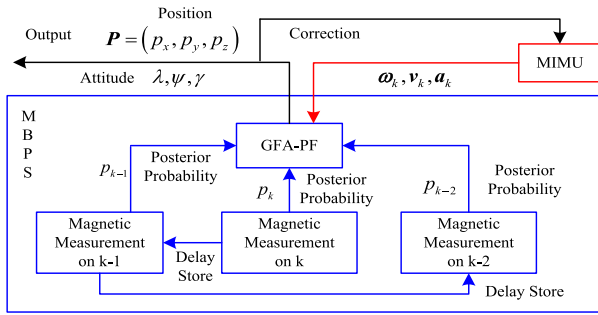$$\omega^{(j)}(t_4) = p_1 \omega^{(j)}(t_3) \quad (34)$$

FIGURE 8. Operational process of the MBPS with the assist of MIMU.

Thus, the weight update relation is

$$\omega^{(j)}(t_4) = p_1 p_2 p_3 \omega^{(j)}(t_1) \tag{35}$$

Herein, the initial weight can be written as

$$\omega^{(j)}(t_1) = \frac{1}{N} \tag{36}$$

Then, using the mini-mental state examination principle and the weight normalization, the state can be computed by

$$x_k = \sum_{j=1}^{N} \omega^{(j)} x_k^{(j)} \tag{37}$$

Assuming 3 MBs can be detected and each of their measurement arrives at t_1, t_2, t_3. Overall, the GFA-PF can be implemented by the following steps:

The operational process can be described in Fig.8. When the measurement arrives at k, the GFA-PF model computes the estimated position and estimated attitude with the posterior probability of $k, k-1, k-2$. With the integration of MIMU, the state of the system is estimated by a particle filter.

IV. RESULTS
In this paper, an advanced MBPS integrated with MIMU was designed to solve the tracking moving target problem considering the time delay case. The feature vector of the very low frequency magnetic field signal was used for the positioning principle, which exhibits better robustness than the intensity method. Therefore, initially, example 1 was used to verify the effective coverage of the proposed MBPS with the very low frequency (10–100 Hz) magnetic field.

A. PARAMETERS OF THE MIMU AND MB IN THE SYSTEM
The MIMU used is the MTi-G-710, which is made by Xsens. As shown in Fig. 9 the accelerometer range is $\pm 20g$, the deviation stability is $40ug$, the gyroscope range is $\pm 450°/s$, and the deviation stability is $10°/h$. Additionally, it can also provide a navigation solution including the velocity output and rotating angle.

The MB parameters are: permeability $\mu = \mu_0 = 4\pi \times 10^2 nT$, $k = 33$, $n = 27$, and $R_d = 7.3cm$, $h_d = 8cm$, and $N_d = 894$ in (4). The MB was excited by a sinusoidal current

Input:

States and weights of receiver position: $\left\{ x_k^{(j)}, \omega_k^{(j)} \right\}_{j=1}^{N}$

Input from MIMU: $\boldsymbol{u}_k(t) = [\boldsymbol{\omega}_k, \boldsymbol{v}_k, \boldsymbol{a}_k]^T$

Output:

Resampled states and weights: $\left\{ \tilde{x}_k^{(j)}, \tilde{\omega}_k^{(j)} \right\}_{j=1}^{N}$

1. Draw starting points of particles based on the IMU:
2. $x_k^{(j)}(t_1) \sim N\left(x_k(t_1), \sigma_x^2(t_1)\right), \omega_k^{(j)} = \frac{1}{N}$
3. **for** $m = 1 : M$ % M is the number of repeated times of one estimation
4.   **for** $j = 1 : N$
5.   Calculate the posterior probability $p_1^{(j)}$ according to (30)
6.   **end**
7.   Estimates $\left\{ x_k^{(j)}(t_2), \omega_k^{(j)}(t_2) \right\}_{j=1}^{N}$ according to (31)
8.   **for** $i = 1 : N$
9.   Calculate the posterior probability $p_2^{(j)}$ at t_2 as (32)
10.   **end**
11.   Estimates $\left\{ x_k^{(j)}(t_3), \omega_k^{(j)}(t_3) \right\}_{j=1}^{N}$ according to (31)
12.   **for** $i = 1 : N$
13.   Calculate the posterior probability $p_3^{(j)}$ at t_3 as (33)
14.   **end**
15.   Update the weights $\tilde{\omega}_k$ based on (35)
16.   Normalization the weights:

$$\tilde{\omega}_k^{(j)} = \frac{\tilde{\omega}_k^{(j)}}{\sum_{i=1}^{N} \tilde{\omega}_k^{(i)}}$$

17.   Determine the central particle of the particles $\left(x_k^{(m)}, \omega_k^{(m)} \right)$ (having the largest weight)
18. **for** $j = 1 : N$
19. Compute the gravitation % **Particles evolution**

$$P = M \cdot dis$$

%where M is the transformation weight based on experience (it is assumed that this is equal to 0.0618 in this paper), dis is the Euclidean distance changing with the central particle.
20. Compute the repulsion

$$Q = f \cdot \sqrt[3]{dis}$$

% The autobiographical factor f is related to dis.
% A very large f contributes to slow convergence.
21.   **if** $abs(dis) < a$
22.   Gravitation $P = 0$
23.   **end**
24.   **if** $abs(dis) > b$
25.   Repulsion $Q = 0$
26.   **end**

27.   % *a* is the gravitation threshold. If *abs* (*dis*) is lower
28.   % than*a*, the gravitation is invalid. Similarly for *b*,
29.   % if *abs* (*dis*) is larger than *b*, the repulsion is invalid
30.   Update each particles according to gravitation and Repulsion:
31.

$$x_k^{(j)} = x_k^{(m)} + P + Q$$

32.   Resampling:
33.   **if** $N_{eff} = \dfrac{1}{\sum\limits_{j=1}^{N} \left(\omega^{(j)}\right)^2} < N_{thr}$ % Here, N_{thr} is the threshold of the effective particle number
34.   **for** $j = 1 : N$
35.   **If** $\omega^{(j)} < \dfrac{1}{N}$
36. $x_k^{(j)} = x_k^{(m)} + \delta_k$
37.   % δ_k is the excitation to keep the variety of particles
38.   **end**
39.   **end**
40.   **end**
41.   **end**
42.   % The number M of repeated times are determined by
        the actual conditions.
43.   % $M = 10$ is defined in the experiment
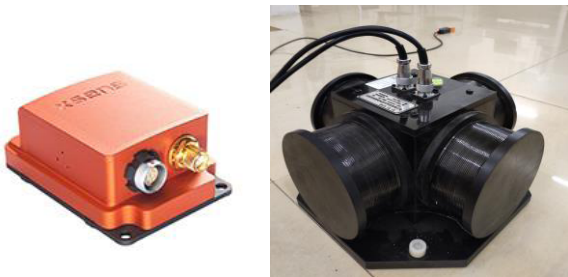44.   State estimation: $x_k = \sum\limits_{i=1}^{N} \omega^{(i)} x_k^{(i)}$

FIGURE 9. The applied MIMU: MTi-G-710 and the designed MB.

$I = 16A$ generated by a digital-to-analog converter with a computer clock and amplified by a power amplifier.

B. EFFECTIVE COVERAGE VERIFICATION

The mutual inductance is linear in the log domain according to the Biot-Savart Law, when the medium and frequency of the magnetic field are constant. The experimental environment is shown in Fig. 10. The frequency of the signal is 20 Hz. The magnetic intensity and distance between the point and the MB are shown in TABLE 1, and the fitting line is shown in Fig. 11.

According to Fig.11, it can be concluded that the fitting (synthetic) line effectively shows the relation between the distance and the magnetic intensity. The mean error of the magnetic intensity is close to 7%. The resolution of the magnetic sensor is 1nT. Obviously, the effective coverage of the
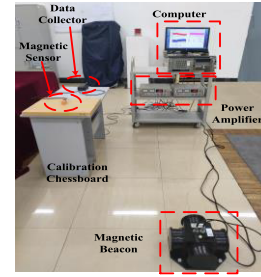

FIGURE 10. Experimental setup (the point is signed by a calibration chessboard, where the length of the grid is 2.3cm).

TABLE 1. Fitting line according to magnetic intensity and distance.

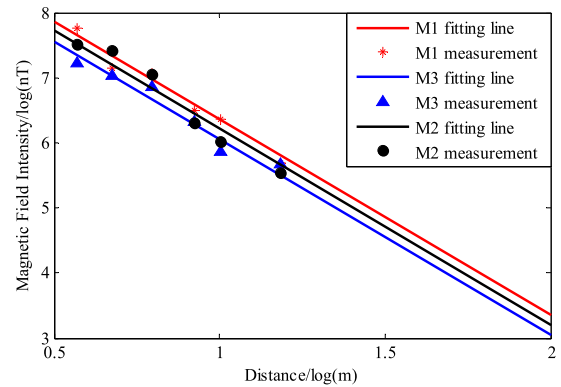|		Magnetic Intensity/dBnT			Synthetic Line
	Position/m	M_1	M_2	M_3	$Y=kx+b$
		(25 Hz)	(20 Hz)	(30 Hz)	
P_1	(0.60, 1.80, 0.50)	7.14	7.03	7.42	$k_1 = -2.995$;
P_2	(0.60, 2.40, 0.50)	6.50	6.32	6.29	$b_1 = 9.353$
P_3	(1.20, 1.20, 0.50)	7.76	7.22	7.50	$k_2 = -3.001$;
P_4	(1.20, 1.80, 0.50)	7.06	6.85	7.04	$b_2 = 9.057$
P_5	(1.20, 2.40, 0.50)	6.36	5.86	6.02	$k_3 = -3.005$;
P_6	(1.20, 3.00, 0.50)	5.68	5.67	5.53	$b_3 = 9.217$

FIGURE 11. Fitting (synthetic) line according to the magnetic line and distance (the result shows that the two parameters are close to a straight line on a logarithmic domain).

system is a combination of four factors, which can be listed as: the decay of the magnetic field, precision of magnetic sensor, the distribution, and the detected quantity of magnetic beacon. The criterion of the effective coverage of the system is positioning accuracy. When the four factors are determined, we can use a posteriori Cramer-Rao Bound [27], such as

$$\mathbf{J}_{k+1} = \mathbf{D}_k^{22} - \mathbf{D}_k^{21} \left[\mathbf{D}_k^{11} + \mathbf{J}_k\right]^{-1} \mathbf{D}_k^{12}$$
$$\mathbf{J}_0 = E\left\{-\Delta_{\mathbf{x}_0}^{\mathbf{x}_0} \log p\left(\mathbf{x}_0\right)\right\} \qquad (38)$$

wherein,

$$\mathbf{D}_k^{11} = E\left\{-\Delta_{\mathbf{x}_k}^{\mathbf{x}_k} \log p\left(\mathbf{x}_{k+1} \,|\mathbf{x}_k\right)\right\},$$
$$\mathbf{D}_k^{12} = -E\left\{\Delta_{\mathbf{x}_k}^{\mathbf{x}_{k+1}} \log p\left(\mathbf{x}_{k+1} \,|\mathbf{x}_k\right)\right\} = \left(\mathbf{D}_k^{21}\right)^T,$$
$$\mathbf{D}_k^{22} = \mathbf{Q}_k^{-1} + \sum_{i=1}^{L} E\left\{-\Delta_{\mathbf{x}_k}^{\mathbf{x}_k} \log p\left(\mathbf{y}_{k+1}^i \,|\mathbf{x}_{k+1}\right)\right\}. \qquad (39)$$

Herein $\mathbf{J}_{k+1}$ presents the Fisher information matrix at time $k + 1$, $\mathbf{Q}_k$ is measurement noise covariance matrix that is
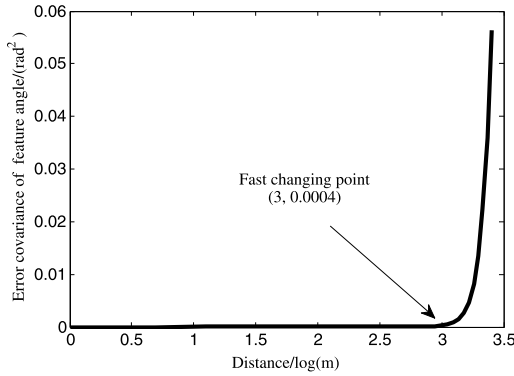
FIGURE 12. The observation covariance of feature angle of the magnetic beacon with increased distance.

affected by the decay of the magnetic field and precision of the magnetic sensor. $p\left(x_{k+1}|x_k\right)$ and $p\left(y_{k+1}^i|x_{k+1}\right)$ are the forecast probability of the system state (position) and the posterior probability of magnetic beacon i at time k, which can be calculated by Equation (20). Normally, the distribution and detected number of the magnetic beacon are constant, once arranged. Therefore, when the magnetic beacon is arranged, the $\mathbf{Q}_k$ can be estimated according to signal-to-noise ratio (SNR) of the observations. According to the requirement of the magnetic beacon model, when the distance from the center of magnetic to the receiver is larger than three times of the size of the magnetic beacon, the model error of magnetic beacon can be ignored [28]. Furthermore, by assuming the resolution of the magnetic sensor as 1nT, the observation covariance of the feature angle of the magnetic beacon with increased distance can be shown by the simulation result (Fig.12).

Therefore, when the magnetic beacon is constant, the effective coverage of one magnetic beacon can be similar to $\exp(3) = 20m$ ideally. Actually, with our experience, the optimal effective coverage is about $1.5m$ to $15m$ in the system. Too small distance leads to a large magnetic beacon model error, and too large one contributes to the larger measured noise for the magnetic field decay, when the three magnetic beacons are located appropriately (angles of each vector point from magnetic to the receiver is larger than 20° and small than 160°). Of course, adding magnetic beacon can improve the performance of the system. It will be presented in the next part.

C. STATIC POSITIONING EXPERIMENT
In this experiment, the magnetic ranging method and the feature vector method proposed in this paper were used for the positioning of a static receiver. The magnetic beacons are located at prior positions and same attitude. The line of sight (LOS) and non-line of sight (NLOS) condition was considered. Initially, three lines acquired in Fig. 11 were determined with the selected frequency and the MB as described. The magnetic ranging method is compared with proposed. The NLOS environments are built by located the receiver behind the wall of concrete structures. With 1000 times
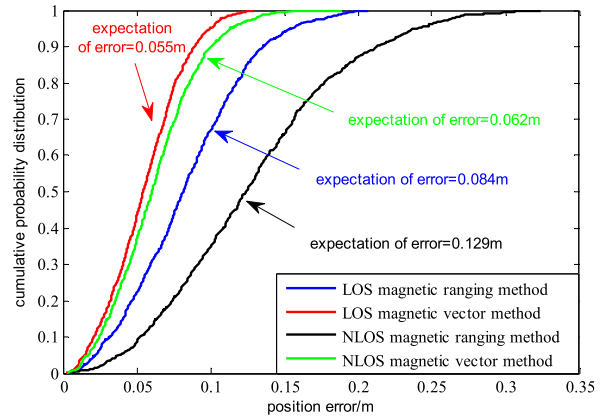

FIGURE 13. The cumulative probability distribution of the positioning error in LOS and NLOS condition for magnetic ranging method and magnetic vector method we proposed. (In the experiments, the expectation of positioning error of magnetic ranging and magnetic vector method in LOS and NLOS condition can be listed as 0.055m, 0.062m, 0.084m and 0.129m).
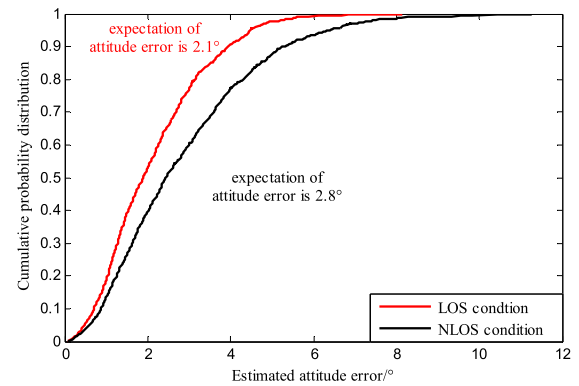

FIGURE 14. The cumulative probability distribution of the estimated attitude error in LOS and NLOS conditions for the proposed method.

Monte Carlo experiments of each condition, the experimental results in LOS and NLOS experiments are shown by the cumulative probability distribution (CPD) in Fig.13.

In Fig. 13, the expected positioning errors with magnetic ranging method in LOS and NLOS conditions are 0.084 m and 0.129 m, respectively. The expected positioning error with the magnetic vector method in LOS and NLOS conditions are 0.055 m and 0.062 m, respectively. The proposed magnetic vector-based method has a better performance than the magnetic ranging method described in an earlier study [12].

Further, the proposed magnetic vector method can realize the estimation of the attitude of the receiver, which can hardly be realized by the magnetic ranging method. According to the principle of attitude estimation, attitude estimation precision is related to the precision of the estimated position. Therefore, the performance of attitude estimation is presented in Fig. 14. With the positioning precision as given in Fig. 13, the expectation of attitude errors in LOS and NLOS conditions can reach 2.1° and 2.8°, respectively.

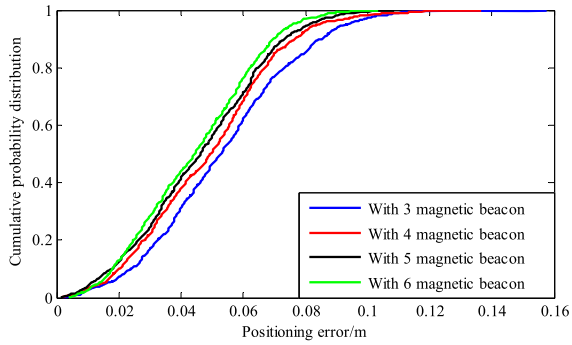Moreover, according to the principle of posteriori Cramer-Rao Bound, quantity higher number of magnetic beacons

FIGURE 15. The cumulative probability distribution of the positioning error in LOS with additional magnetic beacons.

contributes to better performance in the same conditions. In order to verify this assumption, another experiment was done in the same condition as an additional magnetic beacon. The result is shown in Fig. 15. The expectation of the positioning error with 3, 4, 5, and 6 magnetic beacons can be listed as 0.055 m, 0.048 m, 0.046 m, and 0.044 m. Obviously, the increase in the number of magnetic beacons can improve the performance of the system. But considering the limitation of one magnetic beacon for covering it effectively and the cost of the additional magnetic beacons, only four magnetic beacons were found to be appropriate for the most optimum cost and performance.

D. MOVING RECEIVER TRACKING EXPERIMENT

The performance of the proposed method was evaluated by carrying gout an outdoor experiment using the proposed MBPS-MIMU method and the magnetic ranging method combined with MIMU [12]. MIMU-only and MBPS-only configurations were also examined. Four MBs were located at the prior positions $MB_1 = (0m, 0m, 0m)$, $MB_2 = (8.2m, 0.7m, 0.23m)$, $MB_3 = (7.86m, 8.61, 0.11m)$, $MB_4 = (-0.1m, 7.82m, -0.37m)$. The frequency used for each MB was 15, 20, 25, and 30 Hz, respectively. For clarity, all coordinates were transformed based on MB_1. The real position of the receiver was calibrated by a differential GPS (DGPS), whose best precision is 1 cm + 1 ppm. The open outdoor environment ensured that the position result of the DGPS would be very close to the real position. Experimental results are shown in Figs. 16 and 17. The velocity of the receiver was close to 1.2 m/s to 2 m/s.

According to the results, the total running time of the experiment is 18.4s. The trajectories required by the conditions of only using MIMU and only using MBPS are presented by red and green lines, respectively. Loose coupling between MBPS and MIMU is shown by the blue line in Fig. 16. It can be seen easily that the proposed system has the best performance than the two others. With over 800 updating points, the cumulative probability distribution of the positioning error is shown in Fig. 17. According to the result, the two loose coupling systems between MBPS and MIMU described earlier [12] and in this paper perform better than the two sources while working alone. The method in this
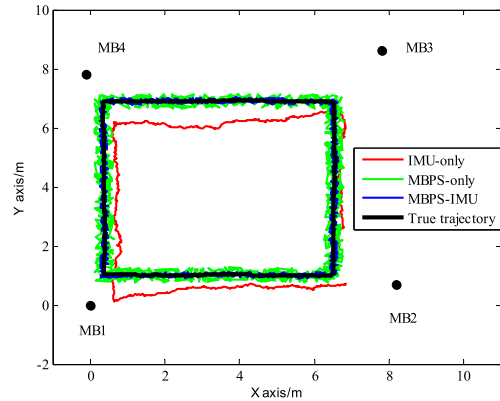

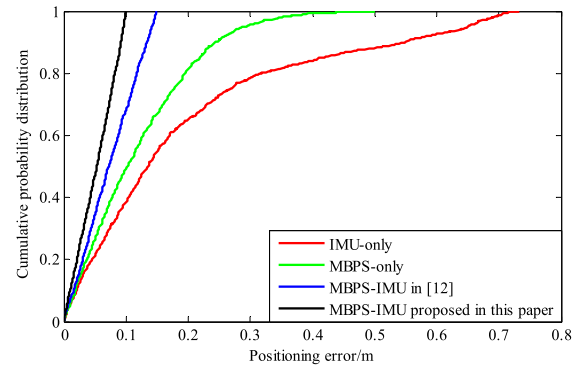**FIGURE 16.** Trajectories obtained by the outdoor experiment.

FIGURE 17. The cumulative probability distribution of the positioning error based on the four methods such as IMU-only, MBPS-only, MBPS-IMU described earlier [12], and MBPS-IMU proposed in this paper.

TABLE 2. Results of MIMU and MBPS-only with different velocities.

Average velocity (m/s)	Error of MBPS-MIMU (m)	Error of MBPS-only (m)
2.3	0.099	0.122
5.2	0.096	0.203
9.6	0.121	0.365
18.7	0.109	0.741

paper shows better performance than the one described in an earlier study [12].

In order to verify the time delay error caused by the velocity, another experiment, which shows the position error of the proposed MBPS integrated with the MIMU, and the MBPS-only with different velocity, was conducted. The parameters are consistent with the previous experiment and the results are shown in TABLE 2.

The results in TABLE 2 indicate that for low velocity conditions, the time delay slightly affects the position accuracy. However, as the velocity increases, the positioning error becomes large. Therefore, by integrating a MIMU on the MBPS, the stability of the MBPS is increased.

V. CONCLUSION

In this paper, an advanced MBPS, which can provide position and attitude information to the receiver, was proposed. The design of an MB model, positioning, attitude principle, optimization method, and a comparison with similar MBPS

were also presented. The error of the MBPS does not accumulate with time and can reach 0.055 m and 0.062 m in the LOS and NLOS environments, respectively, in the static experiment and 0.051 m in the moving target tracking experiment, when integrated with a MIMU. Compared with the magnetic ranging method, the feature vector method does not require the prior magnetic decay environment, which is required in the other method [12]. Thus the proposed method exhibits improved performance and can be widely applied in real cases. The improved robustness of the proposed method was experimentally verified. Furthermore, the proposed method can provide attitude information of the receiver, which is difficult to realize in the intensity method. The non-accumulated error characteristics of the proposed MBPS compensate for the shortage of the MIMU, and the MIMU replenishes the time delay gap, when an MBPS tracking moving target is used. In high-speed conditions, without considering the time delay problem, the estimated error becomes large. The traditional MBPS requires three MBs, which can be detected at the receiver position simultaneously. The proposed system, which is integrated with a MIMU, allows the measurements from different MBs to be separated in the time-axis, which offers a larger working coverage of the MBPS. In addition, the metals in the medium generate the same frequency magnetic field to that of the magnetic beacon. It can be regarded as an additional magnetic beacon with an unknown position. The measured feature vector from the true magnetic beacon will be affected. Furthermore, if there are metals in the environment, the effective coverage of the magnetic beacon will be reduced for absorbing. In this paper, the experimental environment is assumed to be without the effect of metals. The estimation of the effect of metals will be the subject of future investigations.

APPENDIX
Part I: To prove that (5) is monotonous, assume that the derivative of (5) with respect to φ can be described as

$$f'(\varphi) = \frac{g'(\varphi)\, h(\varphi) - g(\varphi)\, h'(\varphi)}{(h(\varphi))^2}\, d\varphi$$

where

$$g(\varphi) = 6r^2 \sin 2\varphi$$
$$h(\varphi) = 4R_d^2 + r^2 + 4h_d^2 + 3r^2 \cos 2\varphi$$

With simplification, it can be described as

$$f'(\varphi) = \frac{48r^2 \cos 2\varphi \left(R_d^2 + r^2 + h_d^2\right) + 36r^4 - 36r^4 \cos 2\varphi}{\left(4\left(R_d^2 + r^2 + h_d^2\right) + 3r^2 \cos 2\varphi - 3r^2\right)^2}$$

It must be

$$\left(R_d^2 + r^2 + h_d^2\right) > r^2$$

Therefore,

$$f'(\varphi) > \frac{12r^4 \left(\cos 2\varphi + 3\right)}{\left(4\left(R_d^2 + r^2 + h_d^2\right) + 3r^2 \cos 2\varphi - 3r^2\right)^2}$$

Because

$$(\cos 2\varphi + 3) > 0, \quad \varphi \in \left(-\frac{\pi}{2}, \frac{\pi}{2}\right),$$
$$f'(\varphi) > 0, \quad \varphi \in \left(-\frac{\pi}{2}, \frac{\pi}{2}\right).$$

The function $f(\varphi)$ is monotonous and the conclusion is proved.

$$f'(\varphi) = \frac{12r^2 \cos 2\varphi \left(4\left(R_d^2 + r^2 + h_d^2\right) + 3r^2 \cos 2\varphi - 3r^2\right)}{\left(4\left(R_d^2 + r^2 + h_d^2\right) + 3r^2 \cos 2\varphi - 3r^2\right)^2}$$
$$+ \frac{6r^2 \sin 2\varphi \left(6r^2 \sin 2\varphi\right)}{\left(4\left(R_d^2 + r^2 + h_d^2\right) + 3r^2 \cos 2\varphi - 3r^2\right)^2}$$
$$= \frac{48r^2 \cos 2\varphi \left(R_d^2 + r^2 + h_d^2\right) + 36r^4 - 36r^4 \cos 2\varphi}{\left(4\left(R_d^2 + r^2 + h_d^2\right) + 3r^2 \cos 2\varphi - 3r^2\right)^2}$$
$$> \frac{48r^4 \cos 2\varphi + 36r^4 - 36r^4 \cos 2\varphi}{\left(4\left(R_d^2 + r^2 + h_d^2\right) + 3r^2 \cos 2\varphi - 3r^2\right)^2}$$
$$= \frac{12r^4 \left(3 + \cos 2\varphi\right)}{\left(4\left(R_d^2 + r^2 + h_d^2\right) + 3r^2 \cos 2\varphi - 3r^2\right)^2} > 0$$

Part II: Prove the assumption: The angle between two feature vectors described in (8) is constant, which is not related to the attitude of the receiver.

According to (9), the feature vector in the coordinate of MB and that of the receiver have the relation

$$v'_i = C_m^r v_i$$

Similarly, it can be obtained that

$$v'_j = C_m^r v_j.$$

The angle $\alpha_{i,j}$ between v_i and v_j can be expressed as

$$\cos\left(\alpha_{i,j}\right) = \frac{(v_i)^T v_j}{|v_i|\,|v_j|} = (v_i)^T v_j.$$

Similarly, $\alpha'_{i,j}$ can be presented as

$$\cos\left(\alpha'_{i,j}\right) = \frac{(v'_i)^T v'_j}{|v'_i|\,|v'_j|} = (v'_i)^T v'_j = \left(C_m^r v_i\right)^T C_m^r v_j.$$

Because C_m^r is the attitude matrix with three-axis rotation, it can be easily know that C_m^r is an orthogonal matrix. Therefore, it has the relation

$$\left(C_m^r\right)^T C_m^r = I_{3\times3}.$$

Finally, it can be easily obtained that

$$\cos\left(\alpha_{i,j}\right) == (v_i)^T v_j = \cos\left(\alpha'_{i,j}\right).$$

The assumption is thus proved.

REFERENCES

[1] K. Aliqab and J. Hong, "UWB balanced BPF using a low-cost LCP bonded multilayer PCB technology," *IEEE Trans. Microw. Theory Techn.*, vol. 67, no. 3, pp. 1023–1029, Mar. 2019.

[2] Z. Yin, X. Jiang, Z. Yang, N. Zhao, and Y. Chen, "WUB-IP: A high-precision UWB positioning scheme for indoor multiuser applications," *IEEE Syst. J.*, vol. 13, no. 1, pp. 279–288, Mar. 2019.

[3] M. Fu, W. Zhu, Z. Le, and D. Manko, "Improved visible light communication positioning algorithm based on image sensor tilting at room corners," *IET Commun.*, vol. 12, no. 10, pp. 1201–1206, Jun. 2018.

[4] C. Tsirmpas, A. Rompas, O. Fokou, and D. Koutsouris, "An indoor navigation system for visually impaired and elderly people based on radio frequency identification (RFID)," *Inf. Sci.*, vol. 320, pp. 288–305, Nov. 2015.

[5] S. H. Kim, S. J. Lee, and S. W. Kim, "Weaving laser vision system for navigation of mobile robots in pipeline structures," *IEEE Sensors J.*, vol. 18, no. 6, pp. 2585–2591, Mar. 2018.

[6] H. Hellmers, Z. Kasmi, A. Norrdine, and A. Eichhorn, "Accurate 3D positioning for a mobile platform in non-line-of-sight scenarios based on IMU/magnetometer sensor fusion," *Sensors*, vol. 18, no. 2, p. 126, Jan. 2018.

[7] J. Blankenbach, A. Norrdine, and H. Hellmers, "A robust and precise 3D indoor positioning system for harsh environments," in *Proc. Int. Conf. Indoor Positioning Indoor Navigat. (IPIN)*, Nov. 2012, pp. 1–8.

[8] A. Norrdine, Z. Kasmi, and J. Blankenbach, "A novel method for overcoming the impact of spatially varying ambient magnetic fields on a DC magnetic field-based tracking system," *J. Location Based Services*, vol. 10, no. 1, pp. 3–15, 2016.

[9] S. Babic, F. Sirois, C. Akyel, and C. Girardi, "Mutual inductance calculation between circular filaments arbitrarily positioned in space: Alternative to Grover's formula," *IEEE Trans. Magn.*, vol. 46, no. 9, pp. 3591–3600, Sep. 2010.

[10] G. De Angelis, V. Pasku, A. De Angelis, M. Dionigi, M. Mongiardo, A. Moschitta, and P. Carbone, "An indoor AC magnetic positioning system," *IEEE Trans. Instrum. Meas.*, vol. 64, no. 5, pp. 1267–1275, May 2015.

[11] M. Dionigi, G. De Angelis, A. Moschitta, M. Mongiardo, and P. Carbone, "A simple ranging system based on mutually coupled resonating circuits," *IEEE Trans. Instrum. Meas.*, vol. 63, no. 5, pp. 1215–1223, May 2014.

[12] V. Pasku, A. De Angelis, A. Moschitta, P. Carbone, J.-O. Nilsson, S. Dwivedi, and P. Handel, "A magnetic ranging-aided dead-reckoning positioning system for pedestrian applications," *IEEE Trans. Instrum. Meas.*, vol. 66, no. 5, pp. 953–963, May 2017.

[13] M. Ortner, M. Ribeiro, and D. Spitzer, "Absolute long-range linear position system with a single 3-D magnetic field sensor," *IEEE Trans. Magn.*, vol. 55, no. 1, pp. 1–4, Jan. 2019.

[14] H. Wu, P. Xu, X. Jiang, and C. Zhang, "High-precision remote ranging with step-frequency-signal magnetic resonance," *IEEE Magn. Lett.*, vol. 9, pp. 1–4, May 2018, Art. no. 1303704.

[15] P. Tang, Z. Huang, and J. Lei, "Fingerprint localization using WLAN RSS and magnetic field with landmark detection," in *Proc. 3rd Int. Conf. Comput. Intell. Commun. Technol. (CICT)*, Ghaziabad, India, Feb. 2017, pp. 1–6.

[16] Y. Chen, M. Zhou, and Z. Zheng, "Learning sequence-based fingerprint for magnetic indoor positioning system," *IEEE Access*, vol. 7, pp. 163231–163244, 2019.

[17] J. Yu, F. Ding, X. Zhao, and F. Zhou, "Error compensation method of magnetometer for attitude measurement using modified artificial bee colony algorithm," in *Proc. 10th Int. Symp. Comput. Intell. Design (ISCID)*, Hangzhou, China, Dec. 2017, pp. 348–351.

[18] H. Huang, J. Zhou, J. Zhang, Y. Yang, R. Song, J. Chen, and J. Zhang, "Attitude estimation fusing quasi-Newton and cubature Kalman filtering for inertial navigation system aided with magnetic sensors," *IEEE Access*, vol. 6, pp. 28755–28767, 2018.

[19] C. Davis, "GPS-like navigation underground," in *Proc. IEEE/ION Position, Location Navigat. Symp.*, May 2010, pp. 1108–1111.

[20] Y. Zong, "A high-precision guidance method of wellbore trajectory based on the rotary magnetic dipole," *Acta Petrolei Sinica*, vol. 32, no. 2, pp. 335–339, 2011.

[21] W. Jia *et al.*, "Magnetic moment direction estimation based on characteristic of magnetic dipole distribution," *J. Detection Control*, vol. 40, no. 2, Apr. 2018.

[22] H. Son and K.-M. Lee, "Distributed multipole models for design and control of PM actuators and sensors," *IEEE/ASME Trans. Mechatronics*, vol. 13, no. 2, pp. 228–238, Apr. 2008.

[23] Y. Wang, "Magnetic-beacon localization technology based on feature vector," Harbin Inst. Technol., Harbin, China, Tech. Rep., Apr. 2018, vol. 40, no. 2.

[24] J. Hu, "Research on the autonomous pedestrian navigation system based on MIMU," Harbin Inst. Technol., Harbin, China, Tech. Rep., Apr. 2018, vol. 40, no. 2.

[25] S.-M. Chen, J. Xiao, H.-Y. Li, and S. Nie, "Particle filter algorithm based on gravitation field," *Control Decis.*, vol. 32, no. 4, pp. 709–714, Apr. 2017.

[26] Y. Qin, *Inertial Navigation*, 3rd ed. Beijing, China: Science Press, 2013, pp. 252–253.

[27] Z. Wang, X. Shen, P. Wang, and Y. Zhu, "The Cramér-Rao bounds and sensor selection for nonlinear systems with uncertain observations," *Sensors*, vol. 18, no. 4, p. 1103, Apr. 2018.

[28] J. B. Nelson, "Calculation of the magnetic gradient tensor from total field gradient measurements and its application to geophysical interpretation," *Geophysics*, vol. 53, no. 7, pp. 957–966, Jul. 1988.
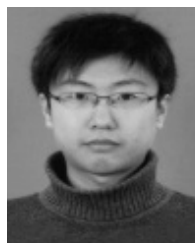
Y. ZHENG received the M.S. and Ph.D. degrees from the Research Center of Space Control and Inertial Technology, Harbin Institute of Technology, in 2014 and 2020, respectively. His research interests include fusion of multi-source data, multi-source navigation and positioning, and optimal selection.
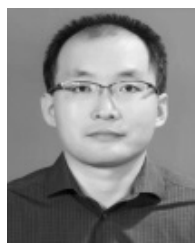
Q. LI received the B.S., M.S., and Ph.D. degrees in control science and engineering from the Harbin Institute of Technology, in 2001, 2003, and 2008, respectively.

Since 2006, he has been with the Research Center of Space Control and Inertial Technology, Harbin Institute of Technology. From 2011 to 2012, he was a Research Assistant with the Department of Aerospace Engineering, University of Michigan. His current research interests include magnetic information navigation, inertial navigation, and motion control.

C. WANG received the B.E., M.S., and Ph.D. degrees in control science and engineering from the Harbin Institute of Technology, Harbin, Heilongjiang, China, in 1983, 1986, and 1991, respectively.

He joined the Department of Control Science and Control Engineering, Harbin Institute of Technology, in 1986, where he is currently a Full Professor. From 1993 to 1994, he was a Postdoctoral Fellow with the Automation Department, Faculté Polytechnique de Mons, Mons, Belgium. He was the Director of control theory and application for a period of five years. He was the Chairman of the Department of Control Science and Control Engineering for a period of three years. He is currently the Deputy Dean of the Academy of Industrial Technology, Harbin Institute of Technology. His research interests include intelligent systems, intelligent control, and network control.

X. LI received the B.S. degree in control engineering from Yanshan University, Qinhuangdao, Hebei, in 2018. He is currently pursuing the M.S. degree in control engineering with the Harbin Institute of Technology, Harbin, Heilongjiang. His research interests include magnetic beacon navigation, pedestrian navigation, and vision-aided inertial navigation.

Y. HUANG received the bachelor's degree in automation from Harbin Engineering University, China, in 2012. Since 2012, he has been working as a Control Engineer with CNNC Nuclear Power Operations Management Company Ltd., Haiyan, China. His current research interests include signal processing, machine learning, and application on control systems.

● ● ●